Chemistry & Biology, Vol. 10, 1173–1181, December , 2003, ©2003 Elsevier Science Ltd. All rights reserved. DOI 10.1016/j.chembiol.2003.11.008

Designer Gene Therapy Using an *Escherichia coli* Purine Nucleoside Phosphorylase/Prodrug System

Eric M. Bennett,[1] Ruchi Anand,[1] Paula W. Allan,[2] Abdalla E.A. Hassan,[2] Jeong S. Hong,[3] Dana N. Levasseur,[5] David T. McPherson,[3] William B. Parker,[2] John A. Secrist III,[2] Eric J. Sorscher,[4] Tim M. Townes,[5] William R. Waud,[2] and Steven E. Ealick[1,*]

[1]Department of Chemistry and Chemical Biology
Cornell University
Ithaca, New York 14853
[2]Southern Research Institute
Birmingham, Alabama 35205
[3]Department of Cell Biology
[4]Department of Medicine
[5]Department of Biochemistry and Molecular Genetics
University of Alabama at Birmingham
Birmingham, Alabama 35294

Summary

Activation of prodrugs by *Escherichia coli* purine nucleoside phosphorylase (PNP) provides a method for selectively killing tumor cells expressing a transfected PNP gene. This gene therapy approach requires matching a prodrug and a known enzymatic activity present only in tumor cells. The specificity of the method relies on avoiding prodrug cleavage by enzymes already present in the host cells or the intestinal flora. Using crystallographic and computer modeling methods as guides, we have redesigned *E. coli* PNP to cleave new prodrug substrates more efficiently than does the wild-type enzyme. In particular, the M64V PNP mutant cleaves 9-(6-deoxy-α-L-talofuranosyl)-6-methylpurine with a k_{cat}/K_m over 100 times greater than for native *E. coli* PNP. In a xenograft tumor experiment, this compound caused regression of tumors expressing the M64V PNP gene.

Introduction

Enzyme-activating prodrug therapy is a recent approach to the treatment of solid tumors [1]. The gene for a drug-activating enzyme is selectively inserted into tumor cells, and a nontoxic prodrug substrate for the enzyme is administered to the patient. Cleavage of the prodrug at the tumor site generates high local concentrations of a toxic drug, which kills tumor cells. For maximum effectiveness, the enzyme/prodrug combination should (a) be specific, so that the prodrug is not a substrate for naturally occurring host enzymes and is cleaved only at the tumor site; (b) use a nontoxic prodrug that can be given in high doses without serious side effects; (c) generate a drug which can cross cell membranes to kill neighboring cells, which did not take up or express the gene ("bystander activity"); and (d) kill both proliferating and nonproliferating cells, to maintain effectiveness against slow-growth tumor cells.

An example of the method is the herpes simplex virus thymidine kinase (HSV-TK)/ganciclovir combination [2], which has been studied in numerous clinical trials [3]. In the treatment of herpes, infected cells always express HSV-TK, and ganciclovir is not a substrate for any mammalian kinase. However, the effectiveness of the HSV-TK method for the treatment of tumors is limited by the difficulty of expressing the gene in a sufficient number of cells, by low bystander activity requiring cell-to-cell contact, and by the lack of activity of the drug ganciclovir triphosphate against nonreplicating cells [4–8].

We have applied molecular design and enzyme redesign ([9–14]; reviewed [15, 16]) to *Escherichia coli* purine nucleoside phosphorylase (PNP) and its natural substrates to create an enzyme/prodrug combination that meets the four criteria listed above for effective gene therapy. PNP catalyzes the reversible phosphorolysis of purine nucleosides or 2′-deoxynucleosides to the free base and sugar phosphate. Human PNP, a homotrimeric enzyme with a total molecular weight of about 100 kDa, is specific for 6-oxopurine nucleosides and has poor activity with 6-aminopurine nucleosides [17]. In contrast, *E. coli* PNP is a homohexameric enzyme with a total molecular weight of about 150 kDa. Differences in the active site (Figure 1A) allow *E. coli* PNP to accept purine nucleosides with 6-oxo, 6-amino, and some nonstandard 6-substituents [18] and also permit it to activate prodrugs that are not substrates for the human enzyme. Systemic treatment with relatively nontoxic adenosine analogs, such as 9-(2-deoxy-β-D-ribofuranosyl)-6-methylpurine (MeP-dR; Figure 1B), has resulted in the selective in vivo killing of ovarian, CNS, hepatoma, and prostate tumors transfected with the *E. coli* PNP gene [19–24]. The liberated base 6-methylpurine (MeP) is highly cytotoxic as a result of its conversion to the nucleoside 5′-monophosphate by adenine phosphoribosyltransferase. Because MeP can pass through cell membranes, transfecting as few as 1% of the tumor cells results in complete bystander killing of nearby tumor cells in culture [25, 26]. However, previous in vivo studies were limited by the maximally tolerated dose (MTD) of MeP-dR that could be administered. Our studies (our unpublished data) indicate that MeP-dR is cleaved by intestinal prokaryotic nucleoside phosphorylases (Figure 2A), increasing the toxicity of this agent: in a study of Black Swiss mice with normal intestinal flora and mice rendered germ free in Trexler isolators [27–29], administration of a known lethal dose (300 mg/kg, QD × 3) of MeP-dR resulted in the death within 6 days of the animals with normal intestinal flora, while two animals that had been rendered germ free showed no weight loss or other ill effects of the test compound and lived for 5 months before being sacrificed. In a second experiment, mice received 2 weeks of treatment with neomycin, streptomycin, bacitracin, and pimaricin to reduce intestinal bacteria and were then challenged with MeP-dR. The LD_{10} of MeP-dR in antibiotic-treated animals

*Correspondence: see3@cornell.edu

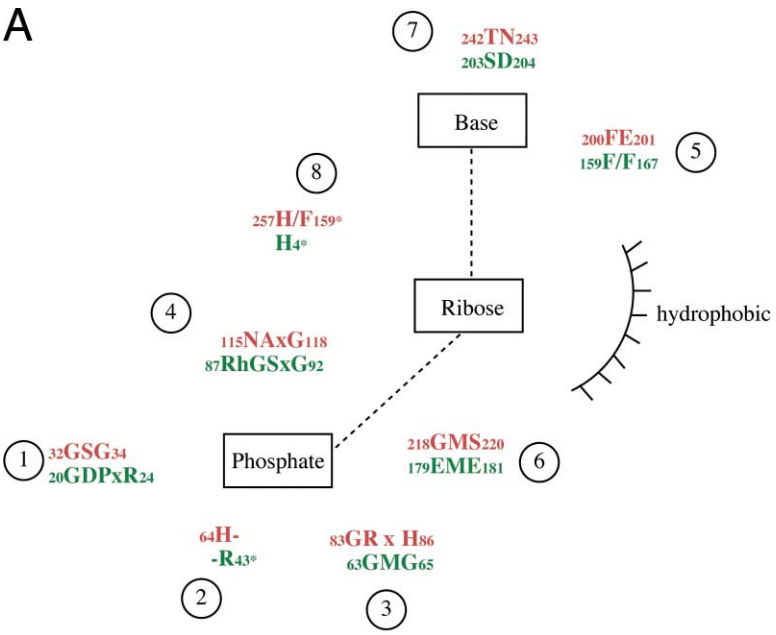

Figure 1. Nucleosides and Their Interaction with the PNP Active Site

(A) Active site structures for *E. coli* PNP and human PNP. Each active site is composed of eight segments. For each segment, the top line, in red, gives the human PNP residue numbers. The bottom line, in green, gives the *E. coli* PNP residue numbers. Segment eight in human PNP comes from an adjacent monomer, and segments two and eight in *E. coli* PNP come from an adjacent monomer (denoted by asterisks). The amino acid residues are aligned based on the structures of the two enzymes. The differences in active site residues result in different substrate specificity, even though the overall fold is the same.

(B) Modified nucleosides used in this study. **1**, 9-(2-deoxy-β-D-ribofuranosyl)-6-methylpurine (MeP-dR); **2**, 9-(6-deoxy-α-L-talofuranosyl)-6-methylpurine [Me(*talo*)-MeP-R]; **3**, 9-(6-deoxy-β-D-allofuranosyl)-6-methylpurine [Me(*allo*)-MeP-R]; **4**, 9-α-L-lyxofuranosyladenine (*lyxo*-Ado); **5**, 9-(5′-5′-di-C-methyl-β-D-ribofuranosyl)-6-methylpurine (5′,5′-dimethyl-MeP-R).

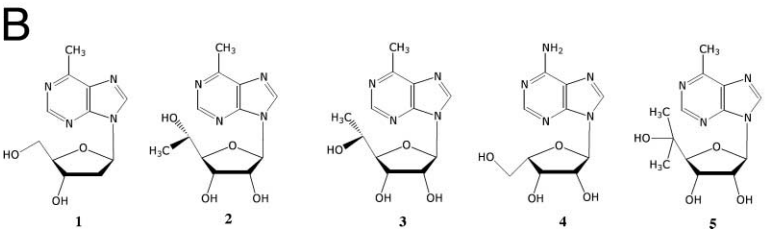

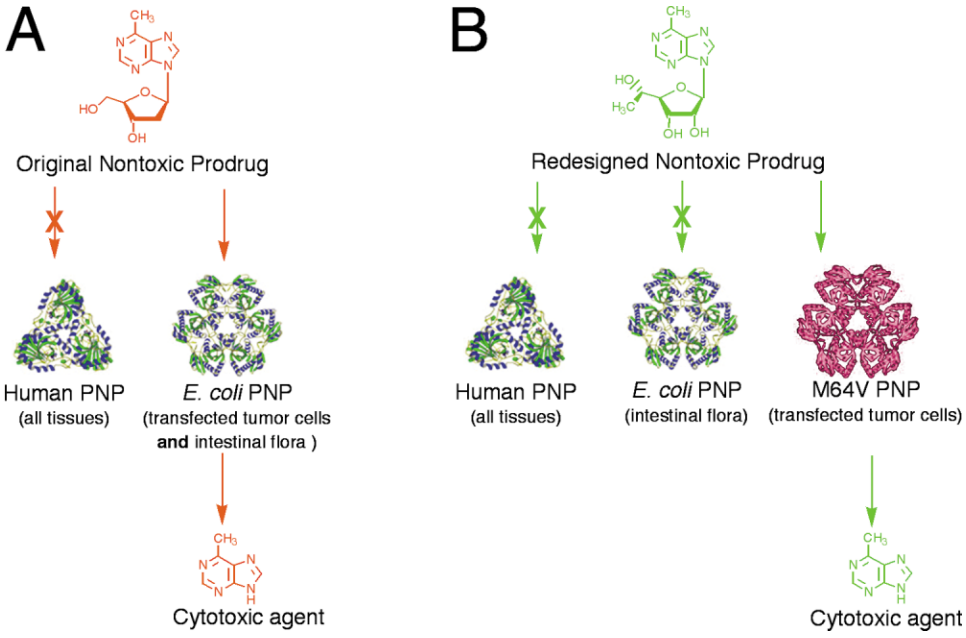

Figure 2. Schematic Representation of Tumor Treatment Using Engineered *E. coli* PNP

Nucleoside prodrugs are relatively nontoxic until activated by cleavage to liberate the free base. Neither of the prodrugs shown is cleaved by human PNP.

(A) The original prodrug (shown in red) is cleaved by wild-type PNP. Because wild-type PNP is present in intestinal flora in addition to transfected tumor cells, cancer treatment using the original prodrug results in systemic toxicity.

(B) The redesigned prodrug (shown in green) is only cleaved by the M64V mutant, thus resulting in cytotoxicity only at the site of the tumor.

Table 1. Specific Activities of Wild-Type and Mutant PNPs

Substrate	Enzyme	Specific Activity (nmol/mg/hr)
MeP-dR	wild-type	740,000
	M64A	11,000
	M64I	190
	M64Q	5100
	M64V	400,000
lyxo-Ado	wild-type	4500
	M64V	43,000
Me(*talo*)-MeP-R	wild-type	960
	M64A	1800
	M64I	20
	M64Q	90
	M64V	68,000
Me(*allo*)-MeP-R	wild-type	110
	M64V	240
5′,5′-dimethyl-MeP-R	wild-type	no activity detected
	M64V	280

(490 mg/kg, QD × 3) was approximately 5-fold higher than it was in nontreated animals. Therefore, to alleviate the toxicity caused by intestinal bacteria, we have redesigned *E. coli* PNP and its prodrug substrate to create a new combination, M64V mutant PNP with 9-(6-deoxy-α-L-talofuranosyl)-6-methylpurine [Me(*talo*)-MeP-R; Figure 1B], in which the prodrug is cleaved only by the enzyme to be delivered to the tumor (Figure 2B).

Results

Kinetic Measurements

Assays with M64A, M64I, M64Q, and M64V mutant *E. coli* PNPs showed MeP-dR cleavage at less than 2% of the wild-type activity, except M64V, for which the relative rate was ~50%. Me(*talo*)-MeP-R activities with M64A, M64I, M64Q, and M64V mutants were 200%, 2%, 10%, and 7000% of wild-type activity, respectively. M64V PNP was also more active than wild-type PNP with other 5′-modified nucleoside analogs, including 9-(6-deoxy-β-D-allofuranosyl)-6-methylpurine [Me(*allo*)-MeP-R, Figure 1B, factor of 2 more active], 9-α-L-lyxofuranosyl-adenine (*lyxo*-Ado, Figure 1B, factor of 9), and 9-(5′-5′-di-C-methyl-β-D-ribofuranosyl)-6-methylpurine (5′,5′-dimethyl-MeP-R, Figure 1B, activity became detectable). Specific activities are summarized in Table 1.

Because Me(*talo*)-MeP-R and *lyxo*-Ado had the greatest activity with M64V PNP, kinetic parameters were determined with these compounds (Table 2). For both substrates, K_m decreased and V_{max} increased by about 10-fold relative to wild-type PNP. The catalytic efficiency (k_{cat}/K_m) with Me(*talo*)-MeP-R increased by approximately 140-fold relative to the wild-type enzyme and achieved approximately 10% of the catalytic efficiency of MeP-dR with the wild-type enzyme. This level of activation was well above the target threshold of MeP liberation previously defined as required for in vivo tumor regressions [22]. The catalytic efficiency of M64V with MeP-dR decreased only a small amount relative to wild-type PNP. The almost 2-fold increase in V_{max} was offset by a 3-fold increase in K_m. Although M64V PNP cleaved Me(*allo*)-MeP-R 2-fold faster than wild-type enzyme, this rate was only 0.4% the rate of cleavage of Me(*talo*)-MeP-R with this mutant enzyme.

Computer Modeling

We inspected the lowest-energy conformations found for each complex and characterized the lowest-energy structure that best satisfied requirements for catalysis. The structures chosen by applying these criteria were the global minima in all enzyme/ligand pairings where the ligand was a good substrate and were not the global minima for pairings where the ligand was a poor substrate.

In the wild-type enzyme models with Me(*allo*)-MeP-R and Me(*talo*)-MeP-R, the global minimum was not the most favorable conformation for catalysis. In the latter case, the sugar atoms moved (likely due to steric interference as shown in Figures 3A and 3B) by 1.0–1.8 Å in the plane of the sugar toward the phosphate. The O5′ atom pointed toward the Phe159 phenyl ring and did not form the hydrogen bond with His4 seen for other substrates. For Me(*allo*)-MeP-R, the situation was similar, but the sugar atom movements ranged from 1.0–2.7 Å, and the stereochemistry change at C5′ caused the O5′ atom to hydrogen bond with Ser90. Higher-energy Me(*allo*)-MeP-R structures (11.5 kJ/mol or more above the global minimum) conformed more closely to catalytic constraints but showed O2′ and O3′ making strong hydrogen bonds to the phosphate, with a weaker O2′-E181 hydrogen bond and no O3′-E181 hydrogen bond (good riboside substrates typically have O2′ and O3′ hydrogen bonds to E181). The O5′-His4 interaction was still missing. Some wild-type/Me(*talo*)-MeP-R conformations showed geometry almost identical to inosine but had energies of at least 5.7 kJ/mol above the global minimum.

In the M64V/Me(*talo*)-MeP-R model, the methyl group, which replaces MeP-dR's pro-S hydrogen on the C5′ carbon atom, occupied a hydrophobic hole created by

Table 2. Kinetic Values with Wild-Type and Mutant PNPs

Substrate	Enzyme	K_m (μM)	V_{max} (nmol mg^{-1} hr^{-1})	V_{max}/K_m	k_{cat} (min^{-1})	k_{cat}/K_m
MeP-dR	wild-type	126	1,460,000	11,400	580	4.6
	M64V	340	2,480,000	7400	990	2.9
Me(*talo*)-MeP-R	wild-type	3000	20,400	7	8	0.0027
	M64V	250	240,000	957	96	0.38
lyxo-Ado	wild-type	1350	38,400	28	16	0.012
	M64V	210	276,000	877	74	0.35

Each value represents the average of at least two separate measurements.

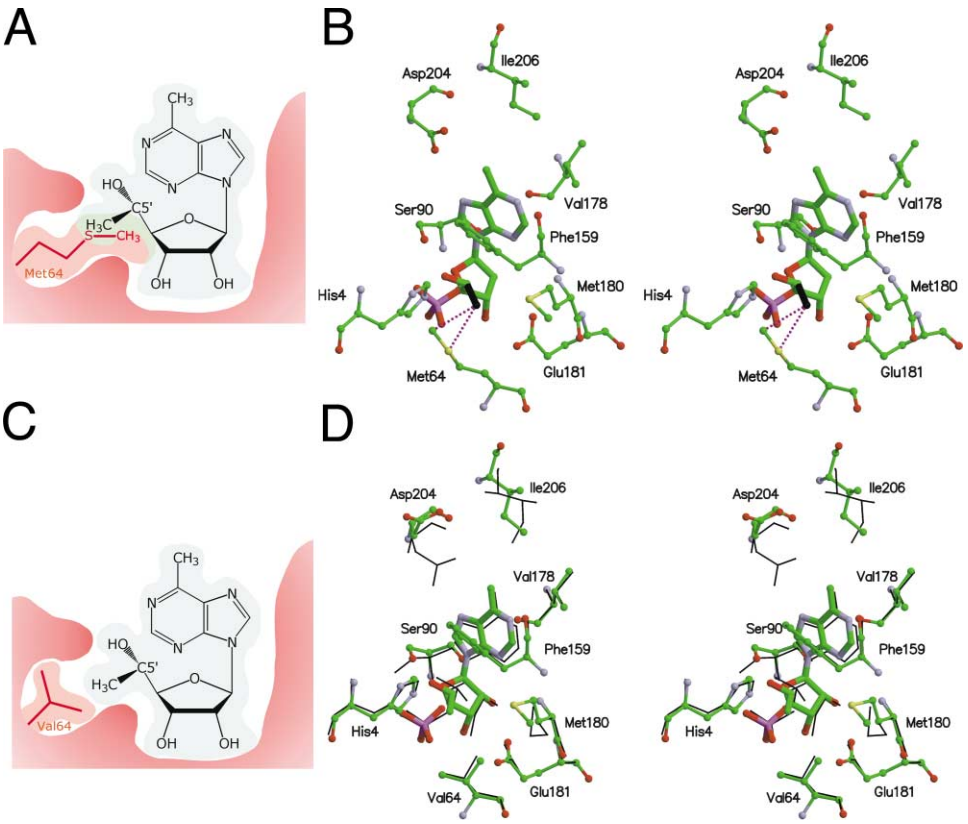

Figure 3. Redesign of PNP to Accommodate a New Prodrug

(A) Modeling studies predicted a steric clash (shown in green) between the 5′-methyl group of Me(talo)-MeP-R and the side chain of Met64.

(B) Stereodiagram of the MeP-dR/wild-type PNP crystal structure (our unpublished data), with crystal structure carbon atoms shown in green. Modeling an additional carbon atom (shown in black) on C5′ results in unfavorable steric interactions (purple dotted lines) with the Met64 side chain.

(C) The unfavorable interaction is eliminated in the M64V PNP.

(D) Crystal structure of Me(*talo*)-MeP-R with M64V PNP, with the global minimum from computational docking overlayed in black wire frame representation. Panels (B) and (D) were created with Molscript [48] and Raster3D [49].

the M64V mutation (Figures 3C and 3D) and bordered by Phe159, Val64, and Ile71. However, replacing the pro-R hydrogen to generate Me(*allo*)-MeP-R did not fill this hole unless the ligand changed conformation. Most of the low-energy structures either showed a C1′-*exo* sugar pucker or showed the C5′-hydroxyl pointing toward the Phe159 phenyl ring rather than His4. A few conformations had appropriate geometry for catalysis but were higher in energy (8.4 kJ/mol or more above the global minimum). These structures were similar to the Me(*talo*)-MeP-R global minimum except for the reversed stereochemistry, which caused the C5′-OH to approach His4 from inside the hydrophobic hole, while the C6′ methyl group was exposed to solvent.

X-Ray Crystallography

Data collection and refinement statistics appear in Table 3. PNP crystallizes with three monomers (designated A, B, and C) per asymmetric unit. Superposition of empty M64V PNP and wild-type *E. coli* PNP [30] showed no significant folding differences. The active sites of the wild-type/Me(*talo*)-MeP-R and wild-type/Me(*allo*)-MeP-R complexes had no major protein conformational changes and showed density only for the base, with moderate displacements from the standard base binding position. The M64V complexes showed $F_o - F_c$ density for the base at 3.0–3.5 σ and for the sugar in the range 2.0–3.0 σ.

Comparison of the M64V/Me(*talo*)-MeP-R structure (Figure 3B) with that of the wild-type/inosine complex revealed rms differences of 0.53 Å for the base and 0.28 Å for the sugar. Slight movements of the base and Asp204 increased the Asp204/N7 interaction distance to 3.5 Å in the A monomer, with a similar conformation in the C monomer. In the B monomer there was no density for the Asp204 side chain. The A monomer had no phosphate bound, and the loop from residues 18 to 25 changed conformation to occupy the phosphate binding site.

In the M64V/Me(*allo*)-MeP-R complex, the nucleoside moved away from Glu181, breaking the O2′ and O3′ hydrogen bonds to Glu181. The movement was in the plane of the Glu181 carboxylate, such that the nucleoside was not bound as deeply in the active site. The displacements were largest (~2.0 Å and ~3.3 Å for O2′ and O3′) in the A and B monomers and smaller (1.4 Å and 1.8 Å) in the C monomer. The O5′ to His4 hydrogen bond was only observed in the C monomer.

In the M64V/MeP-dR structure, ligand binding in the B

Table 3. Summary of Data Processing and Refinement Statistics

Enzyme + Compound	M64V	M64V + MeP-dR	M64V + *talo*	Native + *talo*	M64V + *allo*	Native + *allo*
Refinement resolution (Å)	25–2.7	25–2.2	25–2.3	25–2.5	25–2.4	25–2.5
Unique reflections	28,781	52,262	47,047	37,511	41,133	36,116
Redundancy	10.3	4.3	9.5	8.5	10.0	8.7
Completeness[a]	100 (100)	98.8 (98.7)	100 (100)	100 (100)	100 (100)	100 (100)
R_{sym} (%)[a]	10.0 (22.2)	8.7 (28.7)	10.0 (30.1)	7.6 (26.4)	11.0 (33.2)	7.4 (21.7)
I/σ[a]	6.2 (3.3)	6.5 (2.2)	5.7 (2.4)	7.7 (2.7)	4.5 (2.1)	7.9 (3.3)
R factor (%)	20.6	23.2	22.9	21.5	23.0	21.3
R_{free} (%)	25.1	25.6	25.9	24.5	25.8	24.4
Nonhydrogen atoms	5582	5672	5643	5591	5636	5598
Bond rms deviation (Å)	0.007	0.005	0.007	0.007	0.006	0.006
Angle rms deviation (°)	1.38	1.25	1.34	1.35	1.35	1.35
Avg protein B factor (Å^2)	23.0	26.8	25.9	33.4	24.5	29.7
Avg nucleoside B factor (Å^2)	NA	26.3	35.9	65.7[b]	36.7	49.9[b]

[a] Values for the highest resolution shell are given in parentheses.
[b] Only the purine base was modeled for this complex.

monomer was roughly identical to the binding of inosine (base rms 0.54 Å, sugar rms 0.28 Å) but with a distance of 3.4 Å between N7 and Asp204 and with a slight change in sugar pucker to O4′-*exo*. The A monomer showed significant rms movements of 2.2 Å for the sugar and 2.4 Å for the base. The nucleoside moved, with O5′ as the approximate pivot point, toward a hydrophobic pocket formed by Ala156, Phe159, Tyr160, and Phe167. The C1′-phosphate distance increased to 5 Å as a result. The sugar adopted a C3′-*endo* pucker. The motion in the C monomer was different and smaller in magnitude, with the MeP-dR C8 atom moving to the position of the inosine N7 atom and the sugar moving toward Ser90 by ~0.7 Å. The sugar adopted a C2′-*exo* pucker. In the A monomer, movement of the base broke the hydrogen bond, and a water molecule hydrogen bonded to both the base N7 (3.0 Å) and Asp 204 (2.6 Å). A hydrogen bond between the O5′ oxygen of the sugar and His4 was observed in all three monomers.

In all complexes, the loop region from residue 205 to 220 showed varying disorder for all three monomers.

Biological Studies

The MTD for Me(*talo*)-MeP-R, defined as the maximal dose of a compound that causes less than 15% weight loss and no deaths in mice when administered with a particular route and schedule, was found to be 400 mg/kg/day given ip (intraperitoneally) for 3 consecutive days. D54 cells transfected with the M64V gene were killed with concentrations of Me(*talo*)-MeP-R as low as 20 μM (Figure 4A). Treatment of mice bearing D54 tumors that express M64V showed tumor regression for at least 60 days when treated with Me(*talo*)-MeP-R on 3 consecutive days (Figure 4B).

Discussion

Because intestinal bacteria appear to contribute to the toxicity of MeP-dR, the major goal of this research was to create an antitumor prodrug cleaved only by an engineered PNP and not by enzymes naturally occurring in the host or the intestinal flora. Numerous nucleoside analogs have been screened against the wild-type enzyme [31], and many of the analogs with modifications in the ribose ring were inactive as substrates for *E. coli* PNP (>500,000-fold reduction in activity relative to MeP-dR). Of the nucleosides that were cleaved, Me(*talo*)-MeP-R showed reduced but still significant activity (0.2%) compared to MeP-dR itself. Using the structure of the PNP/MeP-dR complex (our unpublished data) as a template, Me(*talo*)-MeP-R was manually modeled into the active site. Examination of the model suggested that the loss of activity resulted from close contact between the C6′ of Me(*talo*)-MeP-R and the side chain of Met64 (Figures 3A and 3B). To relieve the contact, we modeled other amino acid side chains in place of Met64, and several appeared to create the required space for the additional methyl group (Figures 3C and 3D). Of the experimentally tested mutants, M64V showed the highest increase (100-fold) in processing of Me(*talo*)-MeP-R (Table 1). To further characterize this enzyme/prodrug system, we used crystallography and computer modeling to determine the structures of MeP-dR, Me(*talo*)-MeP-R, and Me(*allo*)-MeP-R (with the opposite stereochemistry at C5′) bound to M64V and wild-type PNP.

The results showed that MeP-dR adopts a conformation similar to that of normal purine nucleoside substrates when bound to PNP, with the largest difference being a change in sugar pucker from C4′-*endo* to O4′-*exo*. The pucker plays a key role in catalysis: if the sugar C1′ atom is above the plane defined by C2′, O4′, and C4′, then, as the glycosidic bond lengthens during formation of the proposed oxocarbenium intermediate, the C1′ atom moves into the C2′-O4′-C4′ plane, satisfying the oxocarbenium planarity requirement. If C1′ is in or below the plane, lengthening of the glycosidic bond conflicts with creating a planar intermediate. The good substrates inosine, adenosine, and MeP-dR all adopt puckers (C4′-*endo* and O4′-*exo*) fulfilling this requirement, while 9-β-D-xylofuranosyladenine, which binds to PNP but is not cleaved, adopts a pucker (C3′-*exo*), which does not (our unpublished data). Xylosides maintain O2′ and O3′ hydrogen bonds to Glu181 as seen in riboside substrates but at the price of a catalytically unfavorable pucker.

In contrast to MeP-dR, ligand electron density for the wild-type/Me(*talo*)-MeP-R complex was disordered,

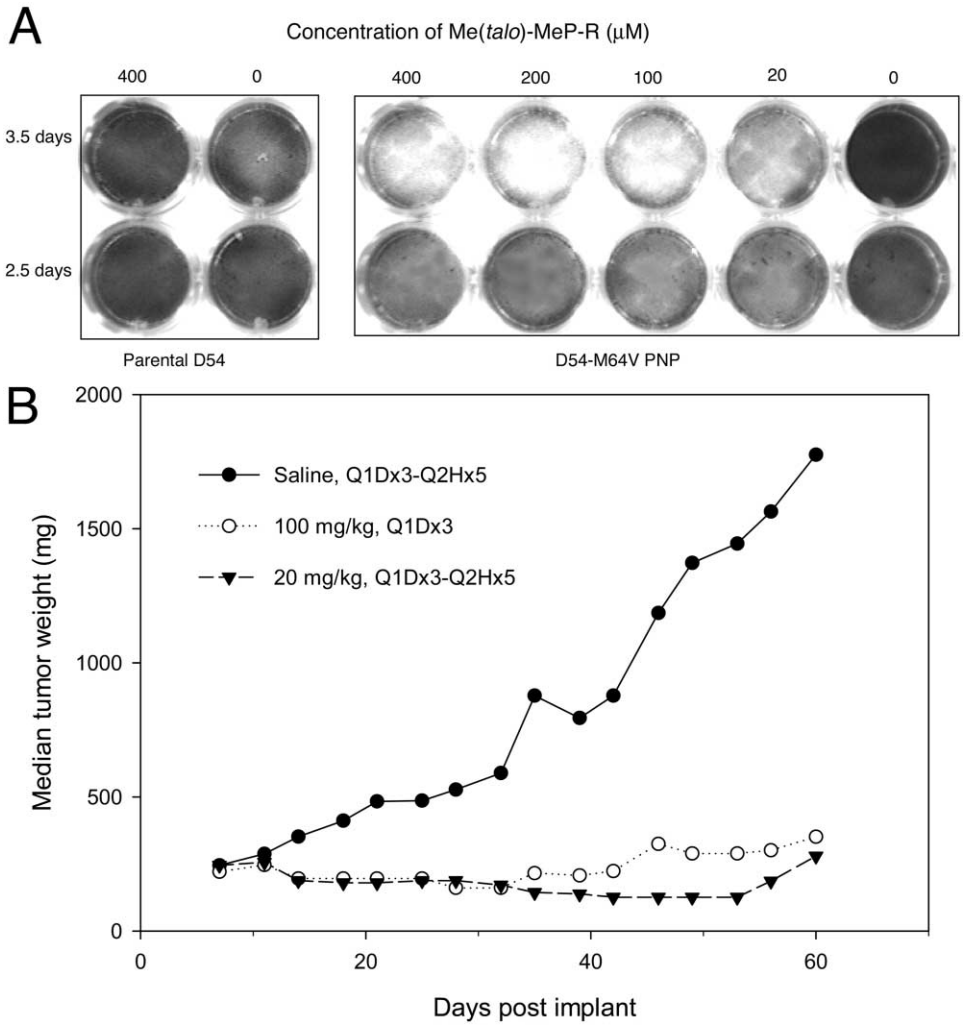

Figure 4. Biological Activity of Me(*talo*)-MeP-R

(A) In vitro cellular activity. The dark stain indicates live cells on the plate, and the clear wells indicate elimination of the cell population. Even at the highest concentration of the compound used (400 mM), parental D54 cells did not exhibit cell death. However, D54-M64V PNP cells died at every concentration of drug tested.

(B) In vivo activity of Me(*talo*)-MeP-R against D54 tumors that express M64V. Mice were treated (ip) with saline (closed circles), 100 mg/kg Me(*talo*)-MeP-R given once a day for 3 days (open circles), or 20 mg/kg of Me(*talo*)-MeP-R given 5 times per day (every 2 hr) for 3 days (closed triangles).

presumably owing to close contacts between C6′ and Met64. Density was only observed in the base binding site. Computer modeling showed that the lowest-energy binding conformations failed to meet one or more criteria for catalysis. Conversely, modeling and crystallography both showed that the M64V mutation created a hydrophobic pocket, bordered by Phe159, Val64, and Ile71, that accommodated C6′, with ligand conformational parameters similar to those seen for other good substrates (Figure 3D). The stereochemistry at the C5′ carbon was critical: the M64V/Me(*allo*)-MeP-R crystal structure showed significantly different binding conformations for the sugar, in which the C1′ atom was 4.4 Å from the nearest phosphate oxygen (too far for effective phosphorolysis) and the C5′-OH moved to form a hydrogen bond with Ser90 rather than His4.

We carried out initial tests of the ability of Me(*talo*)-MeP-R and M64V PNP to kill cells in vitro and in vivo. The prodrug demonstrated poor cytotoxicity against nine non-PNP-transduced human tumor cell lines. The concentration of compound required to inhibit cell growth by 50% was greater than 200 μM in all cases. However, in D54 cells transfected with M64V, Me(*talo*)-MeP-R was able to kill the cells at concentrations as low as 20 μM (Figure 4A). The MTD of Me(*talo*)-MeP-R was approximately 400 mg/kg/day (given ip on 3 consecutive days), which was four times greater than the MTD of MeP-dR (100 mg/kg/day given ip on 3 consecutive days). The difference in the MTD between these two compounds (4-fold) was less than the differences in their catalytic rates with the wild-type enzyme (about 1000-fold), which suggested Me(*talo*)-MeP-R has some other activity in vivo that results in toxicity and limits the amount of compound that could be administered to

mice. Treatment of mice bearing D54 tumors that stably express M64V with Me(*talo*)-MeP-R resulted in excellent antitumor activity (Figure 4B). The maximally tolerated dose of Me(talo)-MeP-R was less in animals bearing D54 tumors that express M64V than it was in non-tumor-bearing animals. All tumors regressed after 3 days of treatment with Me(*talo*)-MeP-R. These results indicate that M64V expressed in vivo is able to cleave Me(*talo*)-MeP-R to generate MeP in the tumor cells and cause their death.

We have shown that enzyme redesign can be used to control prodrug activation by nucleoside phosphorylases. This new enzyme/prodrug combination is directly applicable in a gene therapy approach to tumor cell killing and is the first step in the optimization of the PNP strategy for the treatment of cancer. Further in vivo studies will be needed to fully evaluate the usefulness of Me(*talo*)MeP-R against tumors that express the M64V gene. It is likely that additional improvements will be realized after further cycles of design, analysis, and optimization of treatment.

Significance

Enzyme-activating prodrug therapy is a promising approach to the treatment of solid tumors. A gene encoding an enzyme is introduced into a tumor, and the patient is treated with a nontoxic prodrug, which is converted by the enzyme in the tumor to a toxic, tumor-killing drug. The strategy requires that no naturally occurring enzymes in the host activate the prodrug and that the drug be able to diffuse across cell membranes to kill neighboring tumor cells that failed to take up or express the gene (bystander activity). The herpes simplex virus thymidine kinase (HSV-TK)/ganciclovir combination is one example of the method but is limited by poor bystander activity and inactivity against cells that are not dividing rapidly. Another combination using *E. coli* purine nucleoside phosphorylase with nucleoside prodrugs has shown promise, but the drug doses are limited by toxicity due to cleavage of the prodrug by bacterial nucleoside phosphorylases present in the intestinal flora.

Using crystallographic and computer modeling methods, we have redesigned *E. coli* purine nucleoside phosphorylase and its natural substrates to address the problem of prodrug activation in the digestive tract. The M64V enzyme mutant but not the wild-type enzyme cleaves the prodrug 9-(6-deoxy-α-L-talofuranosyl)-6-methylpurine to generate the toxic drug 6-methylpurine, which has high bystander activity and leads to tumor regression in a mouse model system.

Experimental Procedures

Protein and Ligand Sources

Purified wild-type PNP was a gift from Dr. George W. Koszalka of Wellcome Research Laboratories. Mutant PNPs (M64A, M64V, M64I, M64Q) with a cleavable polyhistidine tail were generated using a kit from Stratagene (La Jolla, California) and purified by standard nickel-affinity techniques.

Me(*talo*)-MeP-R, Me(*allo*)-MeP-R, and 5′-5′-dimethyl-MeP-R were synthesized by condensing MeP with the appropriate blocked carbohydrate [32–34]. *Lyxo*-Ado and MeP-dR were prepared as described [35–37].

Kinetic Data

Enzyme activity was measured in 200 μL volumes containing 50 mM potassium phosphate (pH 7.4), various concentrations of nucleoside, and enough enzyme to give a linear increase in product formation during incubation at 25°C. The reaction was stopped by boiling, and the products were separated from substrate as described [23]. Michaelis-Menten parameters were determined from double-reciprocal plots of 1/velocity versus 1/[substrate]. The best line was determined by linear regression of at least five datum points (regression coefficients were greater than 0.97).

Computer Modeling

Docking studies of MeP-dR, Me(*allo*)-MeP-R, and Me(*talo*)-MeP-R with native and M64V PNP used the GB/SA solvation model [38] and AMBER* force field as implemented in version 7.2 of the program MacroModel [39]. Several generalized ligand angle parameters were adjusted using quantum mechanics calculations at the 6-31G** (geometry optimization) and LMP2/cc-pvtz(-f) (single point energies) levels.

Simulations were based on the structure of the wild-type enzyme complex with inosine (our unpublished results) using a 14 Å shell around the active site. Each nucleoside was positioned in a nonstandard conformation in the binding site and conformational searching was performed using the I-LMOD [40] and MCMM [41] methods to generate trial structures. Residues 4, 64, 90, 159, 180, 203, 204, the ligand, and the phosphate were allowed to move freely, while all other atoms were frozen. The torsions selected for MCMM were $C_\alpha - C_\beta$ and $C_\gamma - S_\delta$ of Met64 and Met180, $C_\alpha - C_\beta$ of Asp204, and C1′-N9 and C4′-C5′ of the ligand. The M64V shell was constructed by manually mutating Met64 to Val. The $C_\alpha - C_\beta$ torsion of Val64 was included in the MCMM torsion list.

Searching was performed until a block of at least 15,000 trial steps resulted in no new structures within 15 kJ/mol of the global minimum. Structures were minimized to a gradient of 0.05 kJ/mol-Å.

Crystallization

PNP was dialyzed into 10 mM KH_2PO_4 buffer at pH 8.0 and concentrated to 35 mg/mL. Hanging drops were prepared by mixing 2 μL of protein with 2 μL 30% ammonium sulfate and 50 mM citrate buffer (pH 5.4). Needle-like crystals appeared within 24–48 hr at room temperature. Wild-type and M64V PNPs crystallized in space group $P6_122$ with approximate unit cell dimensions of $a = 121.6$ Å and $c = 240.0$ Å. Me(*talo*)-MeP-R, Me(*allo*)-MeP-R, and MeP-dR were soaked into the crystals at concentrations of 2–5 mM for 24 hr.

Data Collection and Processing

Crystals were flash-cooled under a 110 K nitrogen stream with a cryoprotectant solution of 20% glycerol in the mother liquor. The data were measured at the A1 and F1 stations at the Cornell High Energy Synchrotron Source in 1° oscillations with exposure times ranging from 20 to 60 s, using a Quantum-4 CCD detector (San Diego Area Detector Systems) with a crystal to detector distance ranging from 200 to 240 mm. Data (60° to 120°) were collected depending on beam time constraints and processed with MOSFLM [42] and SCALA [43].

Structure Determination and Refinement

The structures were solved by molecular replacement with CNS 1.0 [44] and PDB entry 1ECP [30] as a search model. Rigid body refinement, simulated annealing, energy minimization, and individual B factor refinement were performed using CNS with approximately 9% of the reflections reserved to calculate R_{free}. Manual rebuilding was performed with O [45].

Ligand density was visible with M64V mutant PNP for all three compounds. In the wild-type complexes with Me(*talo*)-MeP-R and Me(*allo*)-MeP-R, density was observed only for the purine base, but the entire MeP-dR ligand was observed. A noncomplexed M64V structure was also determined as a control.

Production of Cells Expressing M64V PNP

Lentivirus construction was performed according to the method of Trono et al. [46], using plasmids generously provided by the Trono lab (Geneva, Switzerland). The M64V PNP gene was PCR amplified and subcloned into a Zero-Blunt vector (Invitrogen, Carlsbad, CA). The luciferase gene in the pHR'CMVLuc W Sin-18 lentivirus vector was replaced with PNP. Replacement was verified by sequencing and by using HPLC to detect M64V PNP activity in transfected 293T cells. The transfer vector plasmid was then transfected into 293T cells together with the envelope plasmid pMD.G and packaging construct pCMVDR8.91. Replication deficient viral particles encoding M64V PNP were collected and concentrated 1000-fold by one round of centrifugation at 26,000 rpm for 90 min at 8° using a Beckman SW-28 rotor. Following a 2 hr incubation on ice, the virus was resuspended into serum-free medium. The titer of virus stock was estimated from an enhanced green fluorescence protein (EGFP) lentivirus constructed using the same procedures and an otherwise identical vector backbone. The titer of lentivirus reached 109 infectious particles/mL following concentration. Individual wells of 6-well plates were seeded with 5×10^4 D54MG human glioma cells and infected with recombinant lentivirus. Clonal cells were obtained by limit-diluting the pool of infected cells into 96-well plates and were determined to express active M64V PNP by HPLC and by a conventional cell killing assay in the presence of Me(*talo*)MeP-R in vitro.

Maximally Tolerated Dose Determination

The approximate maximally tolerated dose of Me(*talo*)-MeP-R was determined by administering the compound ip daily for 3 consecutive days at a dose of 400 mg/kg/day to two female athymic nude mice. The mice were monitored for 21 days. A maximum loss in body weight of 15% was observed with no deaths.

In Vitro Cellular Assay

Parental D54 cells (no PNP expression) and D54-M64V PNP (D54 cells stably expressing M64V PNP via lentivirus-mediated transduction) were seeded in 24-well plates. Me(*talo*)-MeP-R was added to D54-M64V PNP cells at concentrations of 0, 20, 100, 200, and 400 μM and to parental D54 cells at concentrations of 0 and 400 μM. The cells were observed daily and then stained with 0.1% crystal violet at 2.5 and 3.5 days following incubation with the compound.

Antitumor Activity Assay

D54/M64V tumor cells (2×10^7) were injected (sc) into the flanks of female athymic nude mice (NCr-*nu*) purchased from Taconic Farms (Germantown, NY). There were six mice in each treatment group and ten mice in the saline-treated control group. The size of the tumors was measured in two dimensions with calipers twice a week, and median tumor weights were determined using the formula for an ellipsoid (length $\times$ width^2/2) and assuming unit density (1 mm^3 = 1 mg) [47]. Therapy with Me(*talo*)-MeP-R began when tumors were approximately 250 mg. Mice were injected ip with saline, 100 mg/kg Me(*talo*)-MeP-R given once a day for 3 days, or 20 mg/kg of Me(*talo*)-MeP-R five times per day (every 2 hr) for 3 consecutive days (Figure 4B).

Acknowledgments

This work used data measured at the Cornell High Energy Synchrotron Source (supported by National Science Foundation award DMR-9311772) using the Macromolecular Diffraction facility (supported by award RR-01646 from the National Institutes of Health). This work was supported by National Cooperative Drug Discovery Grant CA-67763 from the National Institutes of Health. S.E.E. is indebted to the W.M. Keck Foundation and the Lucille P. Markey Charitable Trust.

Received: May 27, 2003
Revised: September 8, 2003
Accepted: September 11, 2003
Published: December 19, 2003

References

1. Xu, G., and McLeod, H.L. (2001). Strategies for enzyme/prodrug cancer therapy. Clin. Cancer Res. *7*, 3313–3324.
2. Culver, K.W., Ram, Z., Wallbridge, S., Ishii, H., Oldfield, E.H., and Blaese, R.M. (1992). In vivo gene transfer with retroviral vector-producer cells for treatment of experimental brain tumors. Science *256*, 1550–1552.
3. Conference briefings. (1999). Hum. Gene Ther. *10*, 3065–3123.
4. Beck, C., Cayeux, S., Lupton, S.D., Dorken, B., and Blankenstein, T. (1995). The thymidine kinase/ganciclovir-mediated "suicide" effect is variable in different tumor cells. Hum. Gene Ther. *6*, 1525–1530.
5. Dennig, C.N., and Pitts, J.D. (1997). Presented at Mol. Cell. Biol. of Gene Therapy, Snowbird, UT, Keystone Symposia.
6. Mesnil, M., and Yamasaki, H. (1997). Presented at Mol. Cell. Biol. of Gene Therapy, Snowbird, UT, Keystone Symposia.
7. Sacco, M.G., Benedetti, S., Duflotdancer, A., Mesnil, M., Bagnasco, L., Strina, D., Fasolo, V., Villa, A., Macchi, P., Faranda, S., et al. (1996). Partial regression, yet incomplete eradication of mammary tumors in transgenic mice by retrovirally mediated HSVtk transfer 'in vivo.' Gene Ther. *3*, 1151–1156.
8. Wygoda, M.R., Wilson, M.R., Davis, M.A., Trosko, J.E., Rehemtulla, A., and Lawrence, T.S. (1997). Protection of herpes simplex virus thymidine kinase-transduced cells from ganciclovir-mediated cytotoxicity by bystander cells: the Good Samaritan effect. Cancer Res. *57*, 1699–1703.
9. Scrutton, N.S., Berry, A., and Perham, R.N. (1990). Redesign of the coenzyme specificity of a dehydrogenase by protein engineering. Nature *343*, 38–43.
10. Clarke, A.R. (1989). From analysis to synthesis: new ligand binding sites on the lactate dehydrogenase framework. Part II. Trends Biochem. Sci. *14*, 145–148.
11. Reeves, C.D., Murli, S., Ashley, G.W., Piagentini, M., Hutchinson, C.R., and McDaniel, R. (2001). Alteration of the substrate specificity of a modular polyketide synthase acyltransferase domain through site-specific mutations. Biochemistry *40*, 15464–15470.
12. Lin, Q., Jiang, F., Schultz, P.G., and Gray, N.S. (2001). Design of allele-specific protein methyltransferase inhibitors. J. Am. Chem. Soc. *123*, 11608–11613.
13. Meng, M., Lee, C., Bagdasarian, M., and Zeikus, J.G. (1991). Switching substrate preference of thermophilic xylose isomerase from D-xylose to D-glucose by redesigning the substrate binding pocket. Proc. Natl. Acad. Sci. USA *88*, 4015–4019.
14. Corbier, C., Clermont, S., Billard, P., Skarzynski, T., Branlant, C., Wonacott, A., and Branlant, G. (1990). Probing the coenzyme specificity of glyceraldehyde-3-phosphate dehydrogenases by site-directed mutagenesis. Biochemistry *29*, 7101–7106.
15. Koh, J.T. (2002). Engineering selectivity and discrimination into ligand-receptor interfaces. Chem. Biol. *9*, 17–23.
16. Penning, T.M., and Jez, J.M. (2001). Enzyme redesign. Chem. Rev. *101*, 3027–3046.
17. Agarwal, K.C., Agarwal, R.P., Stoeckler, J.D., and Parks, R.E., Jr. (1975). Purine nucleoside phosphorylase. Microheterogeneity and comparison of kinetic behavior of the enzyme from several tissues and species. Biochemistry *14*, 79–84.
18. Krenitsky, T.A. (1967). Purine nucleoside phosphorylase: kinetics, mechanism, and specificity. Mol. Pharmacol. *3*, 526–536.
19. Gadi, V.K., Alexander, S.D., Kudlow, J.E., Allan, P., Parker, W.B., and Sorscher, E.J. (2000). In vivo sensitization of ovarian tumors to chemotherapy by expression of *E. coli* purine nucleoside phosphorylase in a small fraction of cells. Gene Ther. *7*, 1738–1743.
20. Martiniello-Wilks, R., Garcia-Aragon, J., Daja, M.M., Russell, P., Both, G.W., Molloy, P.L., Lockett, L.J., and Russell, P.J. (1998). In vivo gene therapy for prostate cancer: preclinical evaluation of two different enzyme-directed prodrug therapy systems delivered by identical adenovirus vectors. Hum. Gene Ther. *9*, 1617–1626.
21. Mohr, L., Shankara, S., Yoon, S.K., Krohne, T.U., Geissler, M., Roberts, B., Blum, H.E., and Wands, J.R. (2000). Gene therapy of hepatocellular carcinoma in vitro and in vivo in nude mice by adenoviral transfer of the *Escherichia coli* purine nucleoside phosphorylase gene. Hepatology *31*, 606–614.

22. Parker, W.B., King, S.A., Allan, P.W., Bennett, L.L., Secrist, J.A., III, Montgomery, J.A., Gilbert, K.S., Waud, W.R., Wells, A.H., Gillespie, G.Y., et al. (1997). In vivo gene therapy of cancer with *E. coli* purine nucleoside phosphorylase. Hum. Gene Ther. *8*, 1637–1644.
23. Parker, W.B., Allan, P.W., Hassan, A.E.A., Secrist, J.A., III, Sorscher, E.J., and Waud, W.R. (2003). Anti-tumor activity of 2-fluoro-2′-deoxyadenosine against tumors that express *E. coli* purine nucleoside phosphorylase. Cancer Gene Ther. *10*, 23–29.
24. Voeks, D., Martiniello-Wilks, R., Madden, V., Smith, K., Bennetts, E., Both, G.W., and Russell, P.J. (2002). Gene therapy for prostate cancer delivered by ovine adenovirus and mediated by purine nucleoside phosphorylase and fludarabine in mouse models. Gene Ther. *9*, 759–768.
25. Hughes, B.W., King, S.A., Allan, P.W., Parker, W.B., and Sorscher, E.J. (1998). Cell to cell contact is not required for bystander cell killing by *Escherichia coli* purine nucleoside phosphorylase. J. Biol. Chem. *273*, 2322–2328.
26. Sorscher, E.J., Peng, S., Bebok, Z., Allan, P.W., Bennett, L.L.J., and Parker, W.B. (1994). Tumor cell bystander killing in colonic carcinoma utilizing the *E. coli* Deo D gene to generate toxic purines. Gene Ther. *1*, 233–238.
27. Coates, M.E. (1968). The Germ-Free Animal in Research (London: Academic Press).
28. Pleasants, J.P. (1974). Gnotobiotics. In Handbook of Laboratory Animal Science, E.C. Melby and N. H. Altman, eds. (Cleveland, OH: CRC Press), pp. 115–174.
29. Trexler, P.C. (1983). Gnotobiotics. In The Mouse in Biomedical Research, H.L. Foster, J.D. Small, and J. G. Fox, eds. (New York: Academic Press).
30. Mao, C., Cook, W.J., Zhou, M., Koszalka, G.W., Krenitsky, T.A., and Ealick, S.E. (1997). The crystal structure of *Escherichia coli* purine nucleoside phosphorylase: a comparison with the human enzyme reveals a conserved topology. Structure *5*, 1373–1383.
31. Secrist, J.A., III, Parker, W.B., Allan, P.W., Bennett, L.L., Waud, W.R., Truss, J.W., Fowler, A.T., Montgomery, J.A., Ealick, S.E., Wells, A.H., et al. (1999). Gene therapy of cancer: activation of nucleoside prodrugs with *E. coli* purine nucleoside phosphorylase. Nucleosides Nucleotides *18*, 745–757.
32. Reist, E.J., Goodman, L., Spencer, R.R., and Baker, B.R. (1958). Potential anticancer agents. IV. Synthesis of nucleosides derived from 6-deoxy-D-allofuranose. J. Am. Chem. Soc. *80*, 3962–3966.
33. Reist, E.J., Goodman, L., and Baker, B.R. (1958). Potential anticancer agents. VIII. Synthesis of nucleosides derived from L-talofuranose. J. Am. Chem. Soc. *80*, 5775–5779.
34. Nutt, R.F., and Walton, E. (1968). Branched-chain sugar nucleosides. II. 5′,5′-Di-C-methyladenosine. J. Med. Chem. *11*, 151–153.
35. Lerner, L.M., Kohn, B.D., and Kohn, P. (1968). Preparation of nucleosides via isopropylidene sugar derivatives. 3. Synthesis of 9-beta-D-gulofuranosyladenine and 9-alpha-L-lyxofuranosyladenine. J. Org. Chem. *33*, 1780–1783.
36. Wnuk, S.F., Yuan, C.S., Borchardt, R.T., Balzarini, J., De Clercq, E., and Robins, M.J. (1997). Anticancer and antiviral effects and inactivation of S-adenosyl-L-homocysteine hydrolase with 5′-carboxaldehydes and oximes synthesized from adenosine and sugar-modified analogues. J. Med. Chem. *40*, 1608–1618.
37. Hassan, A.E.A., Abou-Elkair, R.A.I., Montgomery, J.A., and Secrist, J.A., III. (2000). Convenient syntheses of 6-methylpurine and related nucleosides. Nucleosides Nucleotides Nucleic Acids *19*, 1123–1134.
38. Qiu, D., Shenkin, P.S., Hollinger, F.P., and Still, W.C. (1997). The GB/SA continuum model for solvation. A fast analytical method for the calculation of approximate born radii. J. Phys. Chem. A *101*, 3005–3014.
39. Mohamadi, F., Richards, N.G.J., Guida, W.C., Liskamp, R., Lipton, M., Caufield, C., Chang, G., Hendrickson, T., and Still, W.C. (1990). MacroModel - an integrated software system for modeling organic and bioorganic molecules using molecular mechanics. J. Comput. Chem. *11*, 460–467.
40. Kolossvary, I., and Guida, W.C. (1999). Low-mode conformational search elucidated: application to $C_{39}H_{80}$ and flexible docking of 9-deazaguanine inhibitors into PNP. J. Comput. Chem. *20*, 1671–1684.
41. Chang, G., Guida, W.C., and Still, W.C. (1989). An internal coordinate Monte Carlo method for searching conformational space. J. Am. Chem. Soc. *111*, 4379–4386.
42. Leslie, A.G.W. (1997). MOSFLM Version 5.40 (Cambridge, UK: MRC Laboratory of Molecular Biology).
43. Evans, P.R. (1993). SCALA Version 3.3 (Cambridge, UK: MRC Laboratory of Molecular Biology).
44. Brünger, A.T., Adams, P.D., Clore, G.M., DeLano, W.L., Gros, P., Grosse-Kunstleve, R.W., Jiang, J.S., Kuszewski, J., Nilges, M., Pannu, N.S., et al. (1998). Crystallography & NMR system: A new software suite for macromolecular structure determination. Acta Crystallogr. D Biol. Crystallogr. *54*, 905–921.
45. Jones, T.A., Zou, J.-Y., Cowan, S.W., and Kjeldgaard, M. (1991). Improved methods for the building of protein models in electron density maps and the location of errors in these models. Acta Crystallogr. A *47*, 110–119.
46. Trono, D. (2002). LV'S Kitchen. Trono Lab, www.tronolab.unige.ch/lvkitchen.html.
47. Dykes, D.J., Abbott, B.J., Mayo, J.G., Harrison, S.D.J., Laster, W.R., Simpson-Herren, L., and Griswold, D.P.J. (1992). Development of human tumor xenograft models for in vivo evaluation of new antitumor drugs. Contrib. Oncol. *42*, 1–22.
48. Kraulis, P.J. (1991). MOLSCRIPT: a program to produce both detailed and schematic plots of protein structures. J. Appl. Crystallogr. *24*, 946–950.
49. Merritt, E.A., and Bacon, D.J. (1997). Raster3D: photorealistic molecular graphics. Methods Enzymol. *277*, 505–524.

Accession Numbers

The Protein Data Bank (www.rcsb.org) codes for the *E. coli* purine nucleoside phosphorylase complexes are 1OTY, 1OTX, 1OU4, 1OUM, 1OV6, and 1OVG.